Propagation of spiral waves pinned to circular and rectangular obstacles

Malee Sutthiopad,[1] Jiraporn Luengviriya,[2,3] Porramain Porjai,[1] Metinee Phantu,[1] Jarin Kanchanawarin,[3] Stefan C. Müller,[4] and Chaiya Luengviriya[1,*]

[1]*Department of Physics, Kasetsart University, 50 Phaholyothin Road, Jatujak, Bangkok 10900, Thailand*

[2]*Department of Industrial Physics and Medical Instrumentation, King Mongkut's University of Technology North Bangkok, 1518 Pibulsongkram Road, Bangkok 10800, Thailand*

[3]*Lasers and Optics Research Group, King Mongkut's University of Technology North Bangkok, 1518 Pibulsongkram Road, Bangkok 10800, Thailand*

[4]*Institute of Experimental Physics, Otto-von-Guericke University Magdeburg, Universitätsplatz 2, D-39106 Magdeburg, Germany*

(Received 5 March 2015; published 15 May 2015)

We present an investigation of spiral waves pinned to circular and rectangular obstacles with different circumferences in both thin layers of the Belousov-Zhabotinsky reaction and numerical simulations with the Oregonator model. For circular objects, the area always increases with the circumference. In contrast, we varied the circumference of rectangles with equal areas by adjusting their width w and height h. For both obstacle forms, the propagating parameters (i.e., wavelength, wave period, and velocity of pinned spiral waves) increase with the circumference, regardless of the obstacle area. Despite these common features of the parameters, the forms of pinned spiral waves depend on the obstacle shapes. The structures of spiral waves pinned to circles as well as rectangles with the ratio $w/h \sim 1$ are similar to Archimedean spirals. When w/h increases, deformations of the spiral shapes are observed. For extremely thin rectangles with $w/h \gg 1$, these shapes can be constructed by employing semicircles with different radii which relate to the obstacle width and the core diameter of free spirals.

DOI: 10.1103/PhysRevE.91.052912 PACS number(s): 05.45.−a, 05.65.+b, 82.40.Ck, 82.40.Qt

I. INTRODUCTION

Propagating spiral waves have been discovered in various reaction-diffusion systems such as CO oxidation on platinum surfaces [1], cell aggregation in slime mold colonies [2], electrical wave propagation in cardiac tissues [3], and concentration waves in the Belousov-Zhabotinsky (BZ) reaction [4,5]. In the heart, electrical spiral waves are connected with cardiac tachycardia and life-threatening fibrillations [6,7]. Such spiral waves may cease when their tip hits the boundary of the medium. However, they will survive much longer if they are pinned to anatomical inhomogeneities or obstacles, e.g., veins or scars [3].

Unexcitable disks have been widely taken as model obstacles to study the effects of obstacle size on the properties of spiral waves pinned to them. Tyson and Keener's theoretical work [8] predicted that a spiral wave rotating around a circular hole has period and velocity that increase when the hole is enlarged. Tanaka *et al.* [9] proposed a formula which showed that the spiral wave velocity at the periphery of the circular obstacle increases with the obstacle radius. Simulations by Fu *et al.* [10] revealed that both unexcitable and partially excitable circles cause the period of spiral waves to increase with their radii. Similarly, Cherubini *et al.* [11] showed that the wavelength and the period also increase linearly with the obstacle radius in cardiac model systems, regardless of whether the elasticity of the medium was included in the simulations. For spiral waves in cardiomyocytes, their velocity and wavelength were found to increase linearly with the circumference of the circular obstacle [12].

Experiments using thin layers of the photosensitive ruthenium-catalyzed BZ reaction [13] have demonstrated that wave period, wavelength, and velocity of a spiral wave increased from 26 s, 1.3 mm, and 49.6 μm s^{-1} to 49 s, 3.4 mm, and 74.3 μm s^{-1}, respectively, after an artificial circular core was created by a laser spot of 1.2 mm in diameter. A scroll ring (i.e., a spiral structure in three dimensions) has been often observed to contract and eventually self-annihilate [14,15]. However, the contraction was suppressed when the scroll ring was pinned to spherical plastic beads [16,17].

In this article, we present an investigation of the dynamics of pinned spiral waves in BZ media. We chose two different simple forms of obstacles: circles and rectangles. Circles are symmetric objects which were used in many studies of pinned spiral waves in experiments and simulations, whereas rectangles have the advantage that their width and height are adjustable to obtain different circumferences while the area can be fixed to a constant value. We confirmed our experimental results by numerical simulations using the Oregonator model [18,19].

II. EXPERIMENTS

A. Experimental methods

We prepared the Belousov-Zhabotinsky (BZ) solutions from $NaBrO_3$, H_2SO_4, malonic acid (MA), and ferroin, all purchased from Merck. Stock solutions of $NaBrO_3$ (1 M) and MA (1 M) were freshly produced by dissolving powder in deionized water (conductivity ~ 0.056 μS cm^{-1}), whereas stock solutions of H_2SO_4 (2.5 M) and ferroin (25 mM) were commercially available. To prevent any hydrodynamic perturbation, the reaction was embedded in a 1.0% w/w agarose gel (Sigma). Appropriate volumes of the stock solutions were mixed and diluted in deionized water to form BZ solutions with initial concentrations: $[H_2SO_4] = 160$ mM,

*Corresponding author: fscicyl@ku.ac.th

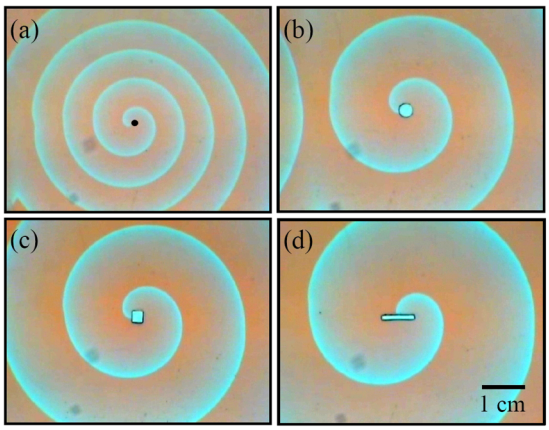

FIG. 1. (Color online) Spiral waves in the BZ reaction: (a) A free spiral wave (no obstacle) with a spiral core of 1.0 mm diameter (black circle), and spiral waves pinned to (b) a circle with diameter 2.8 mm and to rectangles with dimensions (c) 2.3 mm × 2.6 mm and (d) 6.5 mm × 0.9 mm.

[MA] = 50 mM, [$NaBrO_3$] = 50 mM, and [ferroin] = 0.625 mM. At a temperature of 15 °C, the BZ solutions supported spiral waves with wavelength, period, and velocity of 7.5 mm, 11.4 min, and 0.66 mm min^{-1}, respectively.

The influence of unexcitable obstacles on the propagation of spiral waves (shown, e.g., in Fig. 1) was investigated in a uniform thin layer of the BZ reaction using a flat reactor (volume 100 × 100 × 1.0 mm^3) constructed from transparent Plexiglas [20]. Eight circles with different diameters of 1.5, 1.9, 2.5, 2.8, 3.1, 3.5, 3.9, and 4.5 mm and four rectangles with width and height of 2.3 × 2.6, 4.6 × 1.3, 4.9 × 1.2, and 6.5 × 0.9 mm^2 were created also from Plexiglas plates (thickness 1.0 mm, the same as for the BZ layers) using a computerized laser cutting machine [see Figs. 1(b)–1(d) for examples of the obstacles]. The area A and the circumference l of circular and rectangular obstacles are summarized in Fig. 2(a). In each experiment, one obstacle was attached in the reactor before filling in the BZ solution.

A spiral wave pinned to an obstacle was initiated by a two-layer method as demonstrated earlier (cf. Fig. 1 in Ref. [21]). During the observations, the reactor was placed in a transparent thermostatting bath to control the temperature at 15 ± 0.1 °C. The bath was set between a white light source and a color charge-coupled-device camera (Super-HAD, Sony) to record the images of the spiral wave every second with a resolution of 0.10 mm $pixel^{-1}$. The wavelength, the period, and the velocity of spiral fronts were measured at locations at least one wavelength away from the tip of free spirals or from the obstacle edges to which the spirals were pinned to avoid the curvature effect as described in an earlier work [22].

It is worth noting that a difficulty of this experimental investigation comes from the long period of pinned spiral waves and emergences of undesired circular waves and free spirals that are often generated by some sources, like dust particles, in the BZ reaction. Due to their shorter period, these waves, especially the free spirals, interact and subsequently overcome the pinned spiral waves after some time, as mentioned earlier by Steinbock and Müller in Ref. [13]. If such undesired waves occur, by chance, near the obstacles and the structure of pinned spiral wave is perturbed, the measurement criterion described above cannot be fulfilled. In this case, the experiments were repeated with new preparations of the BZ reaction. Therefore, carefully cleaning of the reactor as well as the obstacles before the experiments should be done to minimize the undesired waves.

B. Experimental results

Figure 1 illustrates examples of spiral waves with different wavelengths observed in our experiments. In the absence of obstacles, the BZ solutions supported spiral waves with wavelength λ = 7.5 mm and the spiral tip (measured location as in Ref. [20]) traced a circular area of 1.0 mm in diameter, as in Fig. 1(a). Spiral waves pinned to obstacles having a similar area of about 6 mm^2 but differing in shape and circumference l are shown in Figs. 1(b)–1(d). The wavelength λ was enlarged to 14.3 mm for the case of a circle with diameter 2.8 mm [l = 8.8 mm, Fig. 1(b)]. A similar wavelength (λ = 14.4 mm) was observed for the rectangle with dimensions 2.3 mm × 2.6 mm [l = 9.8 mm, Fig. 1(c)]. The longer rectangle with dimensions 6.5 mm × 0.9 mm [l = 14.8 mm, Fig. 1(d)] resulted in a much larger wavelength of 20.3 mm.

Figure 2 summarizes the properties of pinned spiral waves as well as obstacles investigated in our experiments. Since free spiral waves in the BZ solutions rotated around a circular core with diameter of 1.0 mm, we considered the core as a circular obstacle and included the properties of the free spirals

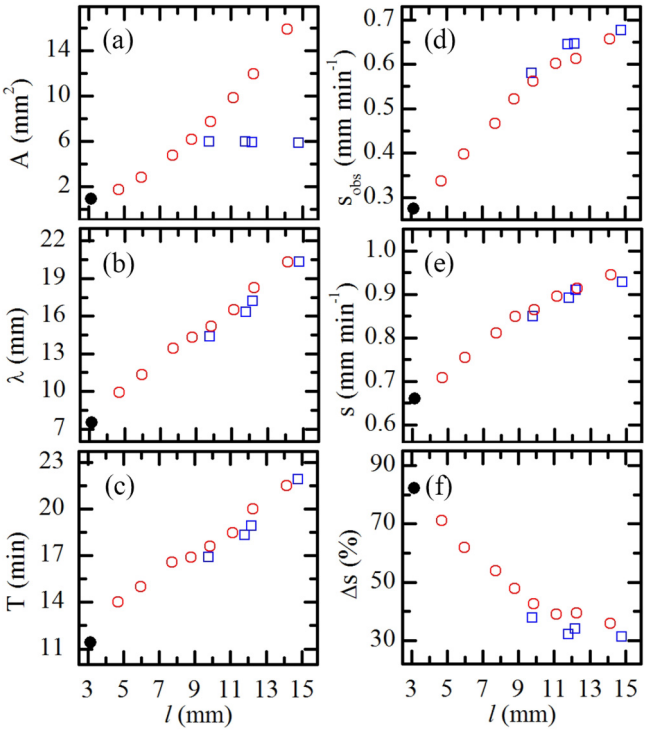

FIG. 2. (Color online) Properties of spiral waves as a function of the obstacle circumference l in the BZ reaction: (a) obstacle area A, (b) wavelength λ, (c) wave period T, [(d) and (e)] velocities s_{obs} and s of waves adjacent to and far from the obstacles, respectively, and (f) percentage difference Δs between s_{obs} and s. Filled circles: no physical obstacles (spiral core diameter 1.0 mm); open circles: circular obstacles; open rectangles: rectangular obstacles.

in Fig. 2 (see filled circles) for the purpose of comparison. Figure 2(a) shows the relation between area and circumference of the obstacles. As the diameter increases from 1.0 to 4.5 mm, the circumference l and the area A of the circles increase simultaneously from 3.1 to 14.1 mm and 0.8 to 15.9 mm^2, respectively. In contrast, the four rectangles (2.3×2.6, 4.6×1.3, 4.9×1.2, and 6.5×0.9 mm^2) with a circumference l ranging between 9.8 and 14.8 mm have almost the same area size of about 6 mm^2.

The spiral waves propagated around the obstacles with wavelength λ [Fig. 2(b)] and wave period T [Fig. 2(c)] increasing with the obstacle circumference l in both the cases of circles and rectangles. Moreover, data points from all obstacles lay approximately on the same line of each graph. The growth rate of the wavelength and the period with respect to the circumference are estimated by linear fits as $\lambda/l = 1.064 \pm 0.043$ and $T/l = 0.806 \pm 0.047$ min mm^{-1}. To investigate the influence of the obstacles on the velocity of the spiral waves, we calculated the average velocity of the wave ends attached to the obstacles s_{obs} as the ratio between the circumference and the period $s_{obs} = l/T$ as well as that of the spiral fronts far away from the obstacles s as the ratio between the wavelength and the period $s = \lambda/T$. As shown in Figs. 2(d) and 2(e), both s_{obs} and s increase with l. Even though s_{obs} is always smaller than s for a given obstacle, its growth rate of s_{obs} ($s_{obs}/l = 0.037 \pm 0.002$ min^{-1}) is larger than that of s ($s/l = 0.024 \pm 0.002$ min^{-1}). Therefore, their percentage difference $[\Delta s(\%) = |s_{obs} - s|/(s_{obs} + s)/2 \times 100]$ becomes smaller, while the circumference increases, as indicated in Fig. 2(f).

The structure of pinned spiral waves is also affected by the obstacles, as shown in Fig 3. During their evolution around circles, the spiral shape remains unchanged all the time and is well fitted by an Archimedean spiral [Fig. 3(a)]. For a rectangle with the width w similar to the height h (i.e., $w/h = 0.9$), the pinned spiral wave still looks similar to an Archimedean spiral [Fig. 3(b)]. When the ratio w/h of the rectangle is increased (i.e., to a more asymmetric shape), the spiral deviates farther from an Archimedean one [e.g., in Fig. 3(c) with $w/h = 7.2$]. In fact, the observed structures differ from any other mathematical spiral known to us (i.e., Euler's, Fermat's, hyperbolic, logarithmic spirals, etc.). These unusual spiral shapes also change periodically, while the waves rotate around the obstacles. As shown in Fig. 3(c), the wave front near the obstacle has a high curvature when the wave end turns around the short boundaries on the left and the right. As the wave end propagates further along the long edges (the upper and the lower walls), the curvature of the nearby front continually decreases. A description of a spiral wave pinned to a rectangle similar to Fig. 3(c), but with extremely high w/h, is given in the section of simulation results (see Figs. 7 and 8).

III. SIMULATIONS

A. Simulation methods

Numerical simulations have been performed using the two-variable Oregonator model, as in Eq. (1), to describe the dynamics of the activator u and the controller v which account for the concentrations of $HBrO_2$ and the catalyst in the BZ reaction, respectively,

$$\begin{aligned} \frac{\partial u}{\partial t} &= \frac{1}{\varepsilon}\left(u - u^2 - f v \frac{u-q}{u+q}\right) + D_u \nabla^2 u, \\ \frac{\partial v}{\partial t} &= u - v + D_v \nabla^2 v. \end{aligned} \tag{1}$$

As in a study by Jahnke and Winfree [19], the parameters were chosen as $\varepsilon = 0.01$, $q = 0.002$, $f = 1.4$, and the diffusion coefficients as $D_u = 1.0$ and $D_v = 0.6$. For this parameter set, the system supported spiral waves with a circular spiral core of 0.9 space units (s.u.) in diameter, wavelength = 10.5 s.u., period = 1.55 time units (t.u.), and velocity = 6.76 s.u. $t.u.^{-1}$.

The variables u and v in Eq. (1) were calculated using an explicit Euler method with a nine-point approximation of the two-dimensional Laplacian operator on a discrete system of a dimensionless size $= 160 \times 160$ s.u. with a uniform grid space of $\Delta x = \Delta y = 0.1$ s.u. and a time step $\Delta t = 3.0 \times 10^{-3}$ t.u., as required for numerical stability [$\Delta t < (3/8)(\Delta x)]^2$ [23]). A single unexcitable circle or rectangle was defined as the obstacle in each simulation. The boundaries of both the medium and the obstacle had no-flux conditions. The implementation of a circular obstacle with no-flux boundary was described in a recent publication [24]. We tested totally 10 circles with different diameters of 1.5, 2.0, 3.0, 4.0, 5.0, 6.0, 7.0, 8.0, 9.0, and 10.0 s.u. and six rectangles with widths

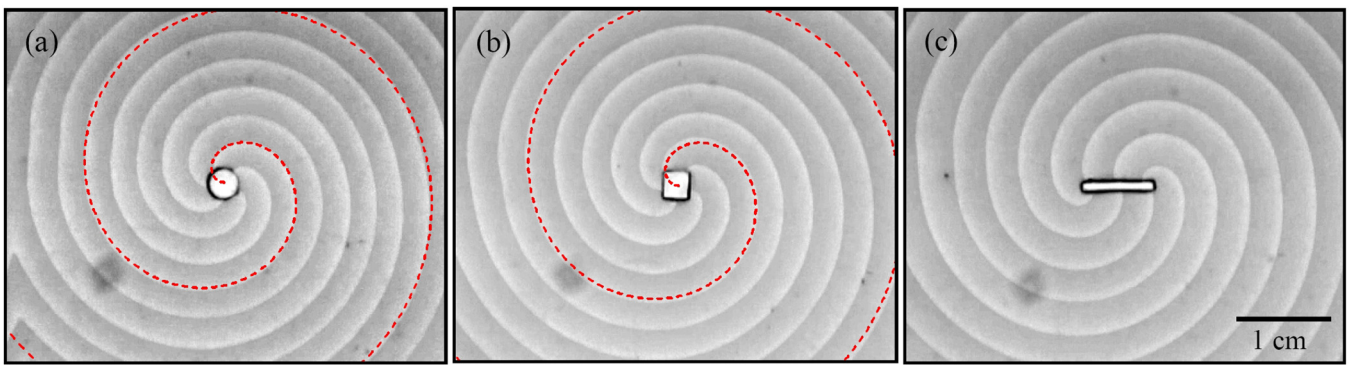

FIG. 3. (Color online) Image overlays of counterclockwise rotating spiral waves pinned to (a) a circle with diameter 2.8 mm and to rectangles with dimensions (b) 2.3 mm × 2.6 mm and (c) 6.5 mm × 0.9 mm in the BZ reaction. Dashed curves in (a) and (b) are Archimedean spirals with origins located at the obstacle centers.

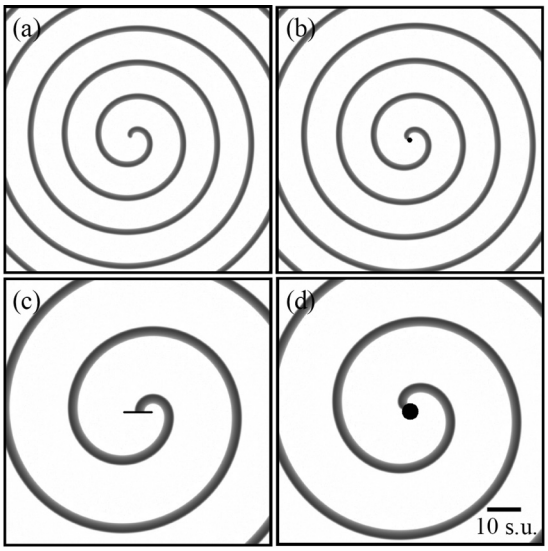

FIG. 4. Spiral waves in the Oregonator model: (a) a free spiral wave (no obstacle, spiral core diameter 0.9 s.u.) and spiral waves pinned to (b) a circle with diameter of 1.5 s.u., (c) a rectangle with dimensions 8.5 s.u. × 0.2 s.u. and (d) a circle with diameter of 5.0 s.u.

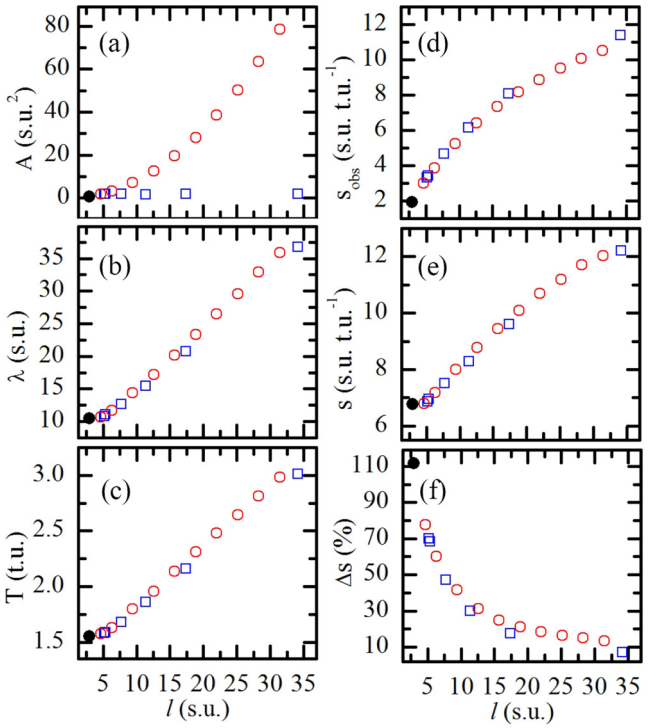

FIG. 5. (Color online) Properties of spiral waves as a function of the obstacle circumference l in the Oregonator model: (a) obstacle area A, (b) wavelength λ, (c) wave period T, [(d) and (e)] velocities s_{obs} and s of waves adjacent to and far from the obstacles, respectively, and (f) percentage difference Δs of s_{obs} and s. Filled circles: no physical obstacles (spiral core diameter 0.9 s.u.); open circles: circular obstacles; open rectangles: rectangular obstacles.

and heights of 1.3 × 1.3, 1.7 × 1.0, 3.4 × 0.5, 5.4 × 0.3, 8.5 × 0.2, and 17.0 × 0.1 s.u.^{2}.

To create a spiral wave pinned to an obstacle, a planar wave was triggered by setting a five-grid-point strip at the left edge of the medium to an excited state (e.g., $u = 1.0$ and $v = 0$ for $0.0 \leqslant x \leqslant 0.5$). When the wave front reached the obstacle (around the middle of the medium), half of the medium was reset to an excitable state (e.g., $u = 0$ and $v = 0$ for $80.0 \leqslant y \leqslant 160.0$), leading to a planar wave with two ends attached to the edges of the obstacle and the system. Subsequently, the wave front curled to form a pinned spiral wave rotating around the obstacle (cf. Fig. 1 in Ref. [21]).

B. Simulation results

Examples of spiral waves with wavelengths depending on the obstacle circumference in the Oregonator model are shown in Fig. 4. A free spiral wave, as in Fig. 4(a), has a wavelength $\lambda = 10.5$ s.u. and its tip rotates around a circular core (diameter 0.9 s.u.). Spiral waves pinned to three different obstacles are shown in Figs. 4(b)–4(d). A small circle with a diameter of 1.5 s.u. (area A = 1.77 s.u.^{2}, circumference $l = 4.7$ s.u.), in Fig. 4(b), caused a small expansion of the wavelength to 10.7 s.u., while a rectangle with dimensions 8.5 s.u. × 0.2 s.u. with a smaller area A = 1.70 s.u.^{2}, but a much longer $l = 17.4$ s.u., in Fig. 4(c), resulted in a spiral wave with a wavelength $\lambda = 20.7$ s.u. In Fig. 4(d), a pinned spiral wave with a wavelength $\lambda = 20.2$ s.u., similar to that in Fig. 4(c), was obtained from a circular obstacle with a diameter of 5.0 s.u. having a similar circumference ($l = 15.7$ s.u.) but much larger area (A = 19.64 s.u.^{2}) in comparison to the rectangle in Fig. 4(c).

The properties of pinned spiral waves and obstacles in our simulations are presented in Fig. 5. As in the experimental part, the free spiral waves were taken as if they were pinned to a circular obstacle with diameter of 0.9 s.u. and their properties were included in this figure (see the filled circles). The obstacle areas A with different circumferences l are shown in Fig. 5(a). For the circular obstacles, the circumference l and the area A increase simultaneously from 3.0 to 31.4 s.u. and 0.71 to 78.55 s.u.^{2}, respectively, when the diameter increases from 0.9 to 10.0 s.u. In contrast, the six rectangles with circumferences l between 5.2 and 34.2 s.u. have similar area sizes of 1.62–1.70 s.u.^{2}. As shown in Figs. 5(b)–5(f), both circular and rectangular obstacles affected the properties of simulated spiral waves in the same manner as found in the experiments. The wavelength λ and the period T increase monotonously with a growth rate of $\lambda/l = 0.921 \pm 0.020$ and $T/l = 0.052 \pm 0.001$ t.u. s.u.$^{-1}$. For a given obstacle, the waves adjacent to the obstacle always propagate slower than the waves far from the obstacle ($s_{obs} < s$) but the rate $s_{obs}/l = 0.288 \pm 0.015$ t.u.$^{-1}$ is larger than $s/l = 0.195 \pm 0.006$ t.u.$^{-1}$. Thus, the percentage difference Δs of the velocities decreases, while the circumference increases.

Figure 6 illustrates examples of spiral structures for different obstacles. For circles and squares (i.e., the ratio of width and height $w/h = 1.0$), the shape of the spiral waves is approximated by Archimedean spirals, as in Figs. 6(a) and 6(b), respectively. For other rectangles with $w/h > 1$, the spiral waves adapt to unusual shapes, which change periodically as observed in our experiments. Figure 6(c) depicts a spiral wave rotating around a rectangle with extremely high w/h of 170. Shortly after the spiral performs a narrow U turn at the left and

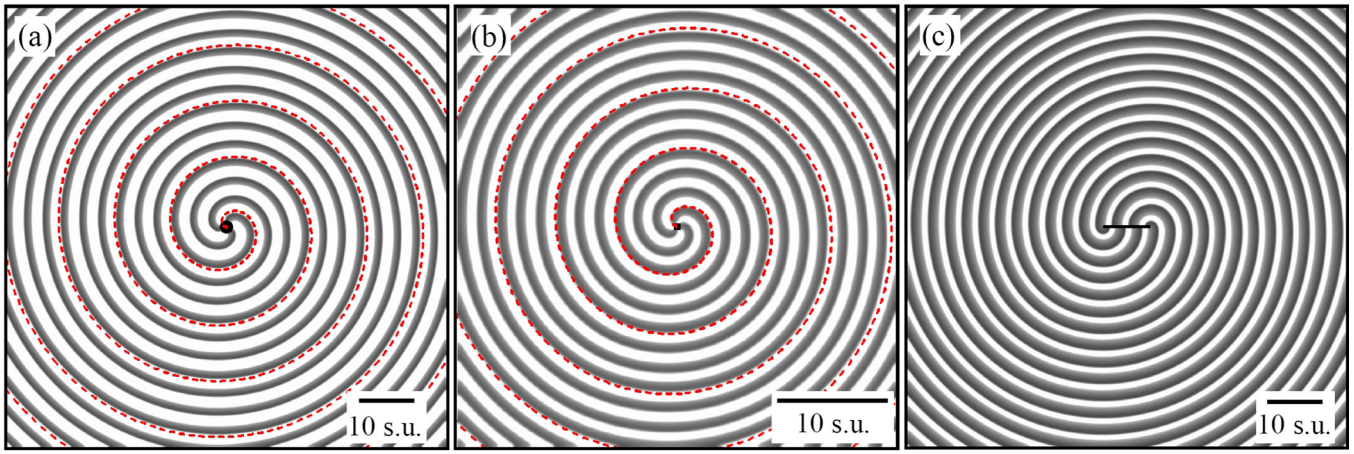

FIG. 6. (Color online) Image overlays of counterclockwise rotating spiral waves pinned to (a) a circle with diameter 5.0 s.u. mm and to rectangles with dimensions (b) 1.3 s.u. × 1.3 s.u. and (c) 17.0 s.u. × 0.1 s.u. in the Oregonator model. Dashed curves in (a) and (b) are Archimedean spirals with origins located at the obstacle centers.

the right ends, the wave front near the obstacle has a very high curvature. Then its curvature decreases, while the wave front traces the horizontal upper and lower walls of the obstacle.

In the following, we consider the spiral shapes in Fig. 6(c), as a first attempt to describe the structures of spiral waves pinned to rectangular obstacles. The overlaid image in Fig. 6(c) is separated into two sections: an upper and a lower half as shown in Figs. 7(a) and 7(b), respectively. Interestingly, they look like two halves of the well-known target patterns, which are often observed in excitable media. All wave fronts in both Figs. 7(a) and 7(b) fit to semicircles, the centers of which are close to (but do not touch) the right and the left boundary of the obstacle, respectively. Figures 7(c)–7(e) show a time series of the segment of a wave front close to the obstacle, while the spiral turns around the right boundary. When the segment reaches the lower right corner, it is almost planar and propagates to the right [Fig. 7(c)]. Shortly afterwards it passes the corner and an additional semicircular front appears [Fig. 7(d)]. Subsequently, the semicircular front expands above the obstacle, as if it is emitted from a point source according to the Huygens principle. The center of the point source is located at a distance $\delta \sim 0.5$ s.u. away from the obstacle wall [Fig. 7(e)]. Note that the distance δ is approximately half of the core diameter of a free spiral wave (0.9 s.u.).

Figure 8(a) illustrates a construction of the structure of the spiral wave with its end moving along the upper boundary of a very thin rectangle (dimensions = 17.0 s.u. × 0.1 s.u.) by using the upper and lower semicircles shown in Figs. 7(a) and 7(b). Starting from the wave end attached to the obstacle, the wave front fits to the upper half of the smallest circle C_0. Then it continues with the lower half of the next circle C_1. Subsequently, the front alternates to the upper half of the circle C_2 and the lower half of the next circle C_3, respectively. In Fig. 8(b), centers and radii of the circles are drawn. The centers of C_0 and C_2 are located close to the right boundary of the obstacle, whereas those of C_1 and C_3 are at the left boundary. The centers are far from the boundary at the same distance ($\delta \sim 0.5$ s.u.). This description is valid for a time interval of about half the rotation period, i.e., during the time that the wave end needs to trace the upper boundary of the obstacle from the right to the left end. Then the wave end turns at the left boundary and a new smallest semicircular wave (new C_0) appears at the lower boundary. This spiral shape can

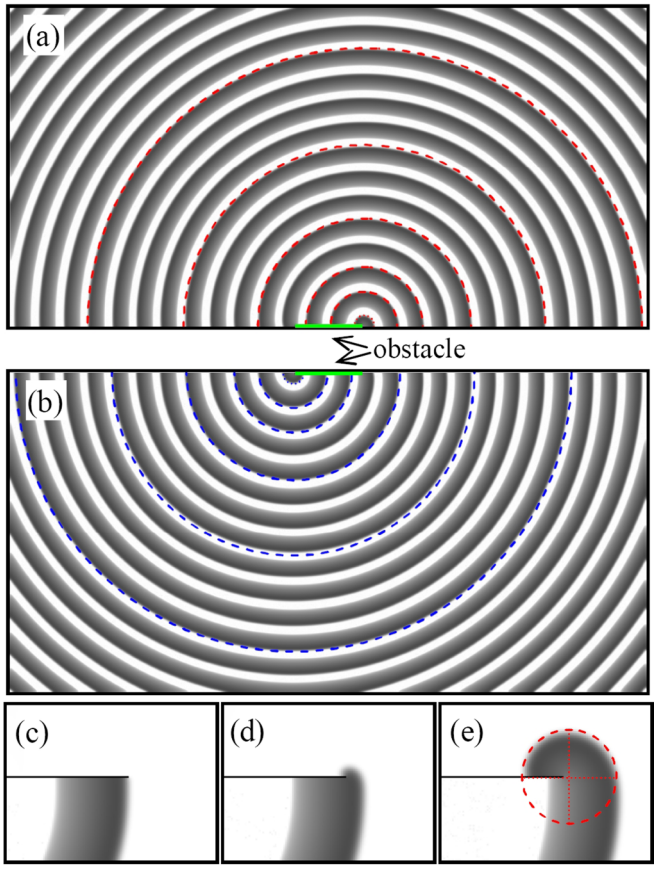

FIG. 7. (Color online) Estimation of the structure of a spiral wave pinned to a very thin rectangle in the Oregonator model. Some wave fronts in (a) the upper and (b) the lower sections of the overlaid image in Fig. 6(c) are compared to semicircles (dashed curves), the centers of which are located close to the right and the left edges of the obstacle. [(c)–(e)] When the wave front turns by an angle of 180° at the right boundary, a semicircular front appears, as if it is produced from a point source [the center of the dashed circle in (e)].

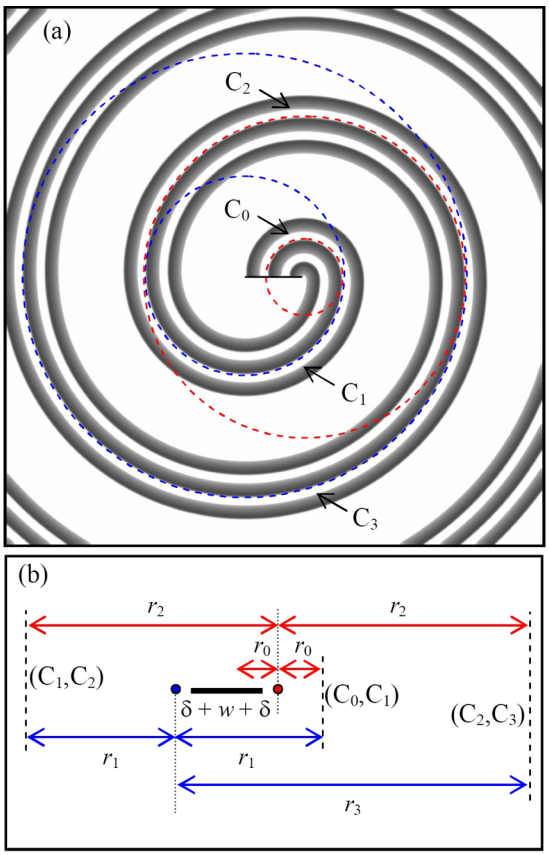

FIG. 8. (Color online) Graphical description of the structure of a spiral wave pinned to a very thin rectangle (black bar) using semicircles. (a) Three consecutive plots of the counterclockwise rotating spiral with the end tracing the upper boundary of the obstacle. The spiral structure at some instant of time can be estimated as a curve that alternately connects upper and lower semicircles of different sizes (corresponding halves of the dashed circles C_0 to C_3). (b) Estimation of the radii r_0 to r_3 of the circles C_0 to C_3 having different centers (two small filled circles) close to the left and the right boundary of the obstacle. For the purpose of illustration, the distance δ is enlarged to a scale different from that of the width w and the radii r_0 to r_3. The vertical dashed lines represent the contact positions of semicircle pairs as indicated by the labels.

be described in the same manner after a reorganization of the circles C_0 to C_3 and their centers.

According to the lifetime of the smallest circle C_0, which is limited to about half of the rotation period as described above, the radius r_0 of the growing C_0 is also limited by the obstacle width w and the distance δ of the circle center: $0 < r_0 \leqslant w + \delta$. It can be clearly seen in Fig. 8(b) that the radii of the larger circles are related to r_0, w, and δ as $r_n = r_0 + n(w + 2\delta)$, where n is an integer.

IV. DISCUSSION AND CONCLUSION

We have presented an investigation of spiral waves pinned to unexcitable obstacles with different sizes and shapes in thin layers of the BZ reaction as well as in simulated systems based on the Oregonator model. Circles with increasing areas and circumferences and rectangles with equal areas but different circumferences were chosen as the obstacles. The results in Figs. 1, 2, 4, and 5 show the common features of the influence of these obstacles on the spiral waves: The pinned spirals propagate with their wavelength, period, and velocity increasing with the obstacle circumference, regardless of the obstacle area. This implies that for such pinning phenomena, the obstacle sizes are more influential due to their circumferences than by their areas.

The time and space units of the simulations are related to the experiments as t.u. $= \mathbf{1/k_5[MA + BrMA]}$ and s.u. $= \sqrt{D/k_5\mathbf{[MA + BrMA]}}$, where the rate of reaction k_5 and the diffusion D of $HBrO_2$ are $0.4\,M^{-1}s^{-1}$ and $1.5 \times 10^{-5}cm^2s^{-1}$, respectively (cf. Ref. [19]). We used [MA+BrMA] $=$ 0.050 M in the experiments so t.u. $=$ 0.83 min and s.u. $=$ 0.27 mm, which results in the core diameter, wavelength, period, and velocity of the free spiral waves as 0.25 mm, 2.88 mm, 1.29 min, and 2.22 mm min^{-1}, respectively. These calculations imply that the excitability in our simulations is relatively higher than that of the real BZ reaction in our experiments, since the simulated spirals had a smaller core diameter, shorter wavelength, shorter period, and higher velocity than for the case of BZ spiral waves. In addition, although our simulations were performed in the excitable regime of the local dynamics [19], we conjecture that pinned spiral waves in oscillatory media would behave in a similar manner. This would hold at least for cases of long period oscillations, because the oscillations will be suppressed by rotating spiral waves with shorter periods, as found in experiments reported earlier [13] as well as in this study.

Tyson and Keener described in Ref. [8] that in determining the angular frequency ω and the asymptotic normal velocity c (at locations far from the hole) of a spiral wave rotating around a hole with radius r_0 in a given medium, the curvature relation (ω as a function of c and r_0) and the dispersion relation (c as a function of ω) must be simultaneously satisfied (see Eq. (24) in Ref. [8]). Both relations are nonlinear and can be solved graphically. Examples for various choices of r_0 in the Oregonator model are given in Fig. 18 of Ref. [8] (a graph of the velocity c versus the period T). It is clear from the intersections of the curves that both the velocity c and the period T of the spiral wave increase simultaneously with the hole radius r_0. The results also imply that the wavelength λ increases with r_0, since $\lambda = c\,T$. Thus, our measurements of both circular and rectangular obstacles shown in Figs. 2, 5(b), 5(c), and 5(e) are consistent with the prediction in Ref. [8], even though it was derived only for the circular case. The necessity of the adjustment of the angular frequency ω due to the presence of a circular hole in the core region of Archimedean spiral waves has been confirmed in a theoretical study by M. Tsoi [25]. Starting from the curvature effect and the methods employed in Ref. [8], Tanaka *et al.* [9] showed that the velocity of a spiral wave at the periphery of a circular obstacle increases with the radius of the obstacle (cf. Eq. (8) in Ref. [9]), which agrees well with our results in Figs. 2(d) and 5(d).

Our present findings show that the proposed theories in Refs. [8,9], which predict how the properties of a pinned spiral wave depend on the radius of a circular obstacle, are also valid for other forms (at least for rectangles) after introducing a small modification in the formulas, e.g., replacing the radius r of the circular obstacle by an equivalent quantity $l/2\pi$ (since $r = l/2\pi$ for a circle), where l is the obstacle circumference.

Circular obstacles have been used in many investigations of the influence of obstacle size on the release of pinned spiral waves. A train of electrical stimuli with a sufficiently high frequency f_{unpin} can induce unpinning of spiral waves. The f_{unpin} increases with the obstacle diameter [9,26–28]. An applied electric field causes reorientation and deformation of ring-shaped filaments of three-dimensional spiral waves (so-called scroll rings) that are pinned to a pair of unexcitable spheres in a BZ solution before the filaments are detached from these spheres [29]. A recent investigation [21] on the unpinning of spiral waves by an applied electrical current in the BZ reaction illustrated that a current with a density higher than a critical value J_{unpin} can release spiral waves pinned to circular unexcitable objects. Similarly to the frequency f_{unpin}, the J_{unpin} increases with the obstacle diameter. Further studies on the unpinning of spiral waves from obstacles with other forms, e.g., rectangles, are suggested to elucidate whether the critical value of the forcing (for instance, the frequency f_{unpin} of the wave train and the critical current density J_{unpin}) relates solely to the obstacle circumference, as in the case for the properties of pinned spiral waves investigated here.

In contrast to the common features of the parameters of propagation in Figs. 2 and 5, the circular and rectangular obstacles result in different shapes of the spiral waves pinned to them. As shown in Figs. 3 and 6, the spirals are similar to Archimedean ones when pinned to circles or rectangles with a width w similar to the height h ($w/h \approx 1$), while the ones pinned to asymmetric rectangles have unusual forms, which also change with time. The structure of a spiral wave pinned to a rectangle with extremely high w/h can be described by using semicircles with radii depending on the width w and the core diameter (2δ) of free spirals, as illustrated in Figs. 7 and 8.

It has been shown earlier that the shapes of free spiral waves with circular cores [30] or those pinned to circular obstacles [31] are comparable to Archimedean spirals. Actually, meandering spiral waves rotating about noncircular cores [22 and references therein] have been more often observed, since they occur in broad ranges of system parameters of excitable media. The structures of these spirals, especially for extremely anisotropic cases like Z-shaped and linear cores [32–35], are complicated and have not yet been analyzed sufficiently. We assume that the structure of spiral waves pinned to a very thin rectangular obstacle, as described in this study, is similar to but simpler than that of free spiral waves with linear cores. While the thin rectangle remains at the same location all the time, the orientation of the linear cores is time dependent (see, e.g., Fig. 6(a) in Ref. [32] and Fig. 1(f) in Ref. [34]). Therefore, the fixed thin rectangular obstacle might be taken as a special case of the linear cores that remain stable or change very slowly in time.

ACKNOWLEDGMENTS

We thank the Department of Physics, the Faculty of Science, the Research and Development Institute (KURDI), the Center for Advanced Studies of Industrial Technology, the Graduate School, Kasetsart University, and the Thailand Research Fund (Grant No. TRG5680044) for financial support.

[1] S. Nettesheim, A. von Oertzen, H. H. Rotermund, and G. Ertl, J. Chem. Phys. **98**, 9977 (1993).
[2] F. Siegert and C. J. Weijer, J. Cell Sci **93**, 325 (1989).
[3] J. M. Davidenko, A. M. Pertsov, R. Salomonz, W. Baxter, and J. Jalife, Nature **335**, 349 (1992).
[4] A. T. Winfree, Science **175**, 634 (1972).
[5] J. Ross, S. C. Müller, and C. Vidal, Science **240**, 460 (1988).
[6] A. T. Winfree, Science **266**, 1003 (1994).
[7] E. M. Cherry and F. H. Fenton, New J. Phys. **10**, 125016 (2008).
[8] J. J. Tyson and J. P. Keener, Physica D **32**, 327 (1988).
[9] M. Tanaka, A. Isomura, M. Hörning, H. Kitahata, K. Agladze, and K.Yoshikawa, Chaos **19**, 043114 (2009).
[10] Y. Q. Fu, H. Zhang, Z. Cao, B. Zheng, and G. Hu, Phys. Rev. E **72**, 046206 (2005).
[11] C. Cherubini, S. Filippi, and A. Gizzi, Phys. Rev. E **85**, 031915 (2012).
[12] Z. Y. Lim, B. Maskara, F. Aguel, R. Emokpae, and L. Tung, Circulation **114**, 2113 (2006).
[13] O. Steinbock and S. C. Müller, Physica A **188**, 61 (1992).
[14] K. I. Agladze, R. A. Kocharyan, and V. I. Krinsky, Physica D **49**, 1 (1991).
[15] C. Luengviriya, S. C. Müller, and M. J. B. Hauser, Phys. Rev. E **77**, 015201 (2008).
[16] Z. A. Jiménez, B. Marts and O. Steinbock, Phys. Rev. Lett. **102**, 244101 (2009).
[17] Z. Jiménez and O. Steinbock, Europhys. Lett. **91**, 50002 (2010).
[18] R. J. Field and R. M. Noyes, J. Chem. Phys. **60**, 1877 (1974).
[19] W. Jahnke and A. T. Winfree, Int. J. Bif. Chaos **1**, 445 (1991).
[20] C. Luengviriya, U. Storb, M. J. B. Hauser, and S. C. Müller, Phys. Chem. Chem. Phys. **8**, 1425 (2006).
[21] M. Sutthiopad, J. Luengviriya, P. Porjai, B. Tomapatanaget, S. C. Müller, and C. Luengviriya, Phys. Rev. E **89**, 052902 (2014).
[22] J. Luengviriya, P. Porjai, M. Phantu, M. Sutthiopad, B. Tomapatanaget, S. C. Müller, and C. Luengviriya. Chem. Phys. Lett. **588**, 267 (2013).
[23] M. Dowle, R. M. Mantel, and D. Barkley, Int. J. Bif. Chaos **7**, 2529 (1997).
[24] J. Luengviriya, M. Sutthiopad, M. Phantu, P. Porjai, J. Kanchanawarin, S. C. Müller, and C. Luengviriya. Phys. Rev. E **90**, 052919 (2014).
[25] M. Tsoi, Persistence of planar spiral waves under domain truncation near the core, Ph.D. thesis, The Ohio State University, 2006.
[26] K. Agladze, M. W. Kay, V. Krinsky, and N. Sarvazyan, Am. J. Physiol. Heart Circ. Physiol. **293**, H503 (2007).
[27] A. Isomura, M. Hörning, K. Agladze, and K. Yoshikawa, Phys. Rev. E **78**, 066216 (2008).
[28] A. Pumir, S. Sinha, S. Sridhar, M. Argentina, M. Hörning, S. Filippi, C. Cherubini, S. Luther, and V. Krinsky, Phys. Rev. E **81**, 010901(R) (2010).
[29] Z. A. Jiménez, Z. Zhang, and O. Steinbock, Phys. Rev. E **88**, 052918 (2013).

[30] S. C. Müller, Th. Plesser, and B. Hess, Physica D **24**, 87 (1987).
[31] J. P. Keener and J. J. Tyson, Physica D **21**, 307 (1986).
[32] V. I. Krinsky, I. R. Efimov, and J. Jalife, Proc. R. Soc. London Ser. A **437**, 645 (1992).
[33] M. A. Dahlem and S. C. Müller, Exp. Brain Res. **115**, 319 (1997).
[34] F. H. Fenton, E. M. Cherry, H. M. Hastings and S. J. Evans, Chaos **12**, 852 (2002).
[35] N. Manz, B. T. Ginn, and O. Steinbock, J. Phys. Chem. A **107**, 11008 (2003).